

pubs.acs.org/acsapm Article

# Graft Semi-Interpenetrating Polymer Network Phase Change Materials for Thermal Energy Storage

Nima Alizadeh, Royall M. Broughton, and Maria L. Auad\*



Cite This: ACS Appl. Polym. Mater. 2021, 3, 1785-1794



ACCESS

Metrics & More

Article Recommendations

Graft Semi-Interpenetrating
Polymer Networks

Acrylic copolymer
OH
Acrylic copolymer
O

ABSTRACT: Graft semi-interpenetrating polymer networks (IPNs) out of poly(ethylene glycol), PEG8000-based polyurethane, and acrylic copolymers were synthesized for phase change applications. The chemical structure of the IPN samples was checked with Fourier transform infrared spectroscopy. Thermal properties of the IPNs were studied using differential scanning calorimetry and thermogravimetric analysis. A scanning electron microscope was used to study the surface morphology of the IPN samples. Moreover, polarized optical microscopy and X-ray diffraction were utilized to examine the crystallization properties of the IPNs. The cycling stability of the IPNs was studied as well. Overall, graft-IPN samples show high thermal and cycling stability with excellent shape solidity and no change in crystallization properties compared to the pristine PEG8000. The results confirm the enormous potential of IPNs in a wide variety of phase change applications.

KEYWORDS: graft semi-interpenetrating polymer networks (IPNs), phase change materials (PCMs), thermal energy storage, polyurethane, acrylic-based copolymers, poly(ethylene glycol) (PEG)

# 1. INTRODUCTION

Phase change materials (PCMs) undergo a phase transition in a narrow temperature range, making them a good candidate for thermal applications. The critical factor for PCMs is their high latent heat, making them capable of thermal energy storage.1 PCMs have a wide variety of applications, including thermal storage and thermal protection. For thermal storage applications, high heat conductivity is required, while for thermal protection, low heat conductivity is desirable. Thermal storage in solar energy; different cooling and heating applications such as ice bank and underground cooling systems; medical applications such as smart packaging for transferring food and medicine; temperature maintenance for buildings, food, and electrical instruments; different military and civil applications such as collectors for microwave antenna in ships and helicopters; and a controlled greenhouse are just a few examples for uses of PCMs. 1,3-13

PCMs are classified into three different kinds based on their transition phase: solid—solid PCMs, solid—liquid PCMs, and liquid—gas PCMs. Solid—solid PCMs are materials where the

crystalline structure changes to another crystalline structure or amorphous phase. Solid—solid PCMs consist of inorganic, organic, and polymer-based PCMs. 14-17

Fatty acids, <sup>18</sup> paraffin waxes, <sup>19</sup> fatty hydrocarbons, <sup>20</sup> fatty alcohols, <sup>21</sup> and poly(ethylene glycol) (PEG) are traditional materials widely used as PCMs. However, all these materials suffer from material leakage, which makes them undesirable for phase change applications. <sup>22</sup>, <sup>23</sup> Therefore, new kinds of methods such as utilizing capsules and copolymerization of polymers were introduced to minimize the leakage in PCM applications. <sup>24</sup>

The essential benefits of polymer-based PCMs compared to traditional PCMs are the absence of leakage, no requirement to

Received: December 9, 2020 Accepted: March 2, 2021 Published: March 12, 2021





Figure 1. (a) Poly-addition polymerization to synthesize linear PU. (b) Free-radical polymerization of the acrylic copolymer. (c) Simple schematic of graft semi-IPN synthesis.

seal, no generation of a gas or liquid, a low-cost and straightforward fabrication process, long cycling stability, and minimum volume change. 12,13,25,26

There are two different types of polymeric solid-solid PCMs. One type consists of a mixture of two polymers where one of the polymers acts as the support with a higher melting point, while the other changes the phase from solid to liquid. Therefore, as long as the supporting polymer does not reach its melting point, the whole system can maintain its structure. This type is called a shape-stabilized PCM.<sup>27</sup> The most significant disadvantage of these materials is the phase segregation after a couple of cycles. 12 The second type of polymeric solid-solid PCMs is synthesized by grafting or copolymerizing two polymers with each other. Overall, low thermal stability, a high transition temperature, and low transition enthalpy were reported as the most important disadvantages of polymeric solid-solid PCMs. Therefore, semi-interpenetrating polymer networks (IPNs) are used as polymeric solid-solid PCMs with excellent stability<sup>28</sup> and high latent heat of fusion for the system. Semi-IPNs benefit from all the advantages of polymeric solid-solid PCMs as well.<sup>28</sup>

Semi-IPN is one kind of polymer blend where one of the polymers is cross-linked. In contrast, the other polymer is linear, making the polymer chains move freely and align in the crystalline structure. <sup>29,30</sup> Two polymers in the IPN structure

are entangled, and it is impossible to separate them without breaking their bonds. Li et al. mentioned that although IPNs show phase separation, these materials exhibit a uniform morphology from forced compatibility due to the structure's physical entanglement.<sup>31</sup> Graft semi-IPN is one kind of IPN system where chemical bonds between two polymers are utilized to increase the compatibility of two polymers and increase the shape stability.<sup>29,30,32,33</sup> IPNs can be classified as simultaneous and sequential IPNs based on the polymerization method. In the sequential process, the first polymer is synthesized while being swollen by monomers of the second polymer. Then, polymerization of the second polymer starts to happen. In simultaneous IPN, polymerization of two polymers occurs together, and there is no interfering reaction between two polymer phases.<sup>29,33,34</sup>

Graft semi-interpenetrating polymer network

Extensive work has been published related to different aspects of IPNs. <sup>23,29,35-37</sup> Various elements affecting the final morphology and properties of IPNs such as the ratio of two polymers, choice of precursors and their ratio, <sup>38,39</sup> diol molecular weight, the polymerization process, <sup>40</sup> utilizing chemical bonds between two polymers, <sup>41,42</sup> and curing profile <sup>38,40,43-45</sup> were investigated. It was concluded that synthesizing graft-IPNs with linear isocyanate enhances the compatibility of two IPNs and therefore improves the final properties. <sup>46-52</sup>

PEG is considered one of the best polymeric materials for PCM applications due to its high latent heat of ~200 J/g, good corrosion resistance, and a wide melting temperature. However, it needs to be sealed in packages to avoid leakage in the system, limiting the opportunities and increasing the final cost of PEG-based PCMs. Hofferent research groups tried to solve the leakage problem of PEG by synthesizing polyurethane (PU) and copolymers out of PEG. Hofferent results suggested high latent heat for synthesized PU with no shape change at high temperatures. Sart et al. Synthesized polystyrene-graft-PEG6000 copolymers for use as PCMs. The results indicated good thermal stability with high latent heat for copolymer samples. It was also suggested that enthalpy increases by an increase in the amount of PEG in the system.

Different research groups utilized PEG in the IPN structure to reach shape stability with high latent heat. Zhang et al. fabricated semi-IPN out of PEG and a gel for phase change applications. Excellent latent heat and shape stability were observed in the synthesized samples.<sup>28</sup>

Sundararajan et al. fabricated PEG-based graft semi-IPN with the simultaneous method. The authors observed enthalpies in the order of 145 J/g.<sup>23</sup> Jiang et al. synthesized graft semi-IPN out of PEG and cellulose diacetate as a support phase. Semi-IPN samples with 90 wt % PEG10000 showed the highest enthalpy of fusion in research.<sup>56</sup> Liu et al. were another research group that synthesized semi-IPN out of PEG/poly(polyethylene glycol diacrylate). The highest heat enthalpy, which was achieved in research, was 117 J/g. All semi-IPN samples showed excellent shape stability as well.<sup>57</sup>

In this research, graft semi-IPN out of PEG8000-based PU and bisphenol A bis(2-hydroxy-3-methacryloxypropyl)ether (BisGMA) and methyl methacrylate (MMA)-based acrylic copolymers were synthesized for the first time. PU acted as the phase-transition material, while the acrylic copolymer acted as a skeleton to keep the whole structure together at high temperature. The polymerization of two phases was studied utilizing Fourier transform infrared (FTIR) spectroscopy analysis. Moreover, the crystallization properties of semi-IPN samples were analyzed using X-ray diffraction (XRD) and polarized optical microscopy (POM). Cycling stability, as one of the essential features of the PCMs, was also examined. Overall, IPN synthesized in this research shows tremendous potential in PCM applications such as solar cells, biomedical and biological containers, heat management for buildings and electronics, the cooling system in the collector of a microwave antenna in ships, and helicopters, among others.

# 2. EXPERIMENTAL SECTION

**2.1. Materials.** Poly(ethylene glycol) (PEG, MW = approximately 8000 g/mol) was purchased from Acros Organics. Hexamethylene diisocyanate (DCH) was received from Tokyo Chemical Industry Co., Ltd. (TCI). Dibutyltin dilaurate (DBTDL) was purchased from Pfaltz & Bauer. MMA and BisGMA were purchased from Acros Organics and Esstech, respectively. Moreover, 2,2'-azobis(2-methylpropionitrile) (AIBN) was purchased from Matrix Scientific. 4 Å molecular sieves, purchased from Alfa Aesar, were used to remove the moisture from MMA and DCH.

**2.2. Methods.** *2.2.1. Synthesis of Graft Semi-IPNs.* PEG8000 was dried before the experiment using an oven. Then, it was melted by transferring into an oil bath at 70 °C.

In a separate container, 20 wt % of BisGMA was dissolved into 80 wt % of MMA. Then, 1 wt % of AIBN based on the total mass of the copolymer was dissolved into the mixture. Afterward, DCH and four

drops of DBTDL were added to the mixture and mixed for 3 min. Finally, the mixture was added to the molten PEG8000 placed in the oil bath at 70  $^{\circ}$ C. Afterward, the mixture was transferred to closed glass molds and cured at 80  $^{\circ}$ C for 6 h. A simultaneous polymerization method was followed to synthesize the graft-IPN system as two polymers do not follow interfering reactions. Figure 1 shows the chemical reactions of graft semi-IPN samples.

As shown in Figure 1, PEG and DCH follow the poly-addition polymerization to synthesize linear PU. Extra isocyanate also reacts with hydroxyl groups of BisGMA to make bonds between two polymers. PU is a polymer phase with high latent heat to fulfill requirements in phase change applications. Monomers in the acrylic copolymer, however, follow free-radical polymerization to make a cross-linked acrylic copolymer. The acrylic copolymer acts as a support to maintain the original form of IPN at a temperature higher than PEG's melting point. The final product is graft semi-IPN with chemical bonds between two polymer phases. Five different IPN samples with varied PU and acrylic copolymer compositions were synthesized, where numbers behind IPN indicate the wt % of PU in the IPN system. For instance, IPN90 has 90 wt % of PU.

2.2.2. Characterization. A Nicolet 6700 FTIR spectrometer from Thermo Scientific (USA) in the attenuated total reflection infrared mode was utilized to study the FTIR spectra of the synthesized samples. FTIR analysis was performed within the 400–4000 cm<sup>-1</sup> wavenumber range with 64 scans and a 4 cm<sup>-1</sup> resolution.

A differential scanning calorimetry (DSC) experiment was performed on a TA Instruments DSCQ2000. Approximately 5-10 mg of the sample was tested each time. The sample was first equilibrated at 0 °C for 5 min, and then, the temperature was increased to 150 °C to remove any thermal history in the samples, followed by decreasing the temperature to 0 °C, and finally brought back to 150 °C all with a 5 °C/min heating rate in a nitrogen atmosphere. The second heat was utilized to determine the thermal properties of the IPN samples. Three replicas were tested for each sample to confirm the validity of the results. Equation  $1^{58}$  was used to calculate the percentage of crystallinity

$$\chi_{\rm c}(\%) = \frac{\Delta H_{\rm m}}{\Delta H_{\rm m}^0} \times 100 \tag{1}$$

where  $\chi_c$  is the crystallinity percentage,  $\Delta H_m$  is the enthalpy of fusion of the IPN sample, and  $\Delta H_m^0 = 196.8 \text{ J/g}^{58}$  is the enthalpy of fusion for totally crystalline PEG.

XRD analysis was performed on a Proto manufacturing powder diffraction system having a Cu K $\alpha$  source with a 1.54 nm wavelength, 40 kV, and 30 mA. Approximately 500 mg of samples in the powder form was tested in the range of  $2\theta$  within 15–40° with around 15 min scan time. The Scherrer formula <sup>59</sup> (eq 2) was utilized to calculate the mean size of crystallites in IPN samples

$$L = \frac{K\lambda}{\beta \cos \theta} \tag{2}$$

where  $\lambda$  is the wavelength of the X-ray source in nanometers (0.15406 nm); K is the Scherrer constant, which is related to the crystallite shape (generally taken as 0.9);  $\beta$  is the diffraction peak width at half-maximum height in radians;  $\theta$  is the peak positions in radians; and L is the average crystallite size.

An Olympus BH-2 polarized optical microscope with a FMA050 digital camera was utilized to study the samples' crystalline morphology. IPN samples were cured between two micro slides to reach the thin, consistent thickness for all the samples.

A Zeiss EVO 50 variable-pressure scanning electron microscope with digital imaging and energy-dispersive spectroscopy was used to study the surface morphology of the fractured samples. Samples were immersed in liquid nitrogen and then were broken to make a brittle failure in samples and avoid fracturing of the samples below their glass transition, which could alter the surface morphology, and fractured surfaces were utilized for scanning electron microscopy (SEM) imaging. The samples were sputter-coated with an EMS 550X auto

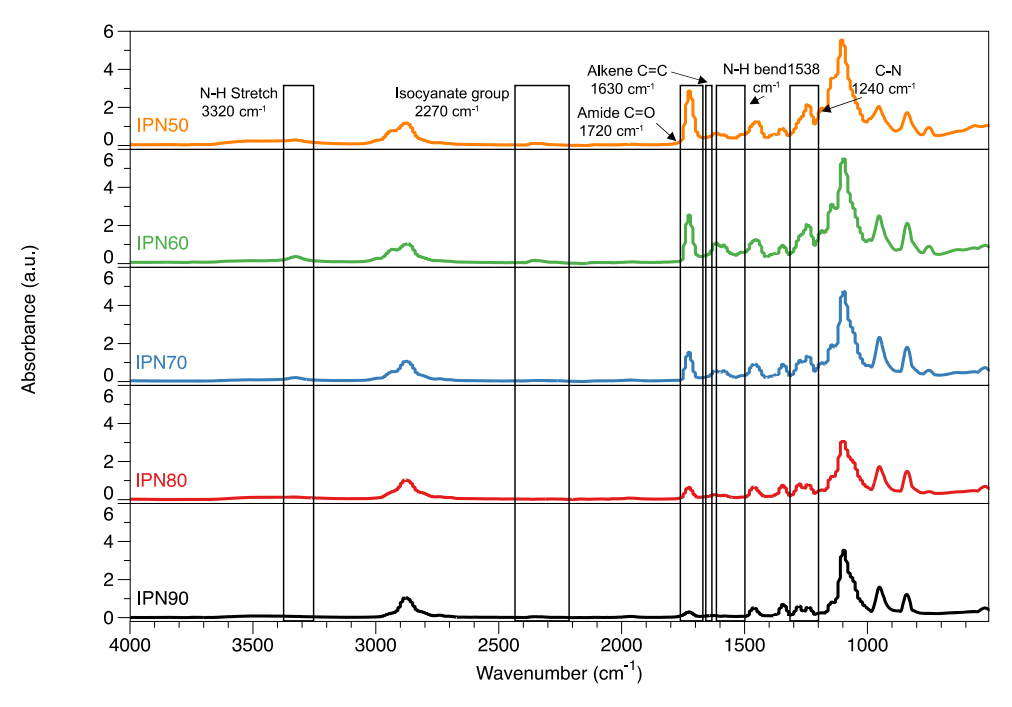


Figure 2. FTIR spectra of IPN samples with different compositions.

sputter coating device with carbon coating attachment before SEM imaging.

Samples were cut to circles with a 12 mm diameter using a Boss Laser LS 3655 and kept in a hot plate at 80  $^{\circ}$ C for 30 min to test the shape stability of the IPN samples.

Thermogravimetric analysis (TGA) was performed under a nitrogen atmosphere using a platinum pan on a TA Instruments TGAQ500. 10–20 mg of samples was heated from room temperature to 800 °C with 10 °C/min.

The thermal cycling stability of the IPN samples was studied by placing the samples into glass vials and then transferring to an oven at 90 °C for 20 min, followed by 20 min in a refrigerator at 10 °C to make sure that solid—liquid—solid transition occurs in the system. The phase-transition cycle was done 25 times. Then, DSC, TGA, FTIR, XRD, and wetting experiments were performed on thermal-cycled samples.

The contact angle of 1.5  $\mu$ L of ultrapure water (UPW) with the IPNs' surface was monitored for 20 s using a DataPhysics OCA 50 instrument. The reported results are the average contact angles of UPW with at least four different IPN samples areas. A Thermo Scientific Barnstead Nanopure (18.2 M $\Omega$ -cm) system was employed to deionize and purify the water. The measurement was analyzed using SCA 20 software.

#### 3. RESULTS AND DISCUSSION

**3.1. Chemical Structure Analysis.** FTIR analysis was utilized to confirm the successful polymerization of two phases

Table 1. Summary of DSC Results for IPN Samples

sample	enthalpy of fusion $(\Delta H_{\rm m})$ $(J/g)$	melting temperature $(T_m)$ (°C)	enthalpy of crystallization $(\Delta H_c)$ $(J/g)$	crystallization temperature $(T_c)$ (°C)
PEG8000	196.0	61.8	198.2	43.6
IPN90	177.5	59.9	174.3	43.9
IPN80	140.3	59.8	141.4	44.2
IPN70	108.7	59.9	105.1	43.3
IPN60	78.1	58.9	74	38.6
IPN50	47.7	54.4	41.3	33.7

in graft semi-IPN. Values on the *Y*-axis were normalized based on the peak at 2880 cm<sup>-1</sup>. Figure 2 shows the FTIR spectra for all of the samples after polymerization. As shown, a peak at approximately 3320 cm<sup>-1</sup> indicates the stretching of the N–H bond due to PU formation in the IPN structure. No peak was observed at around 2270 cm<sup>-1</sup>, which corresponds to the isocyanate bond and confirms the isocyanate consumption to synthesize PU.<sup>60</sup> The peak at about 1720 cm<sup>-1</sup> is attributed to amide C=O, the peak at 1240 cm<sup>-1</sup> belongs to the C–N bond, and the peak at about 1538 cm<sup>-1</sup> corresponds to the N–H bond. These signals are evidence of the successful polymerization of PU. Moreover, there is no peak at approximately 1630 cm<sup>-1</sup>, which belongs to the alkene C=C bond, indicating successful free-radical polymerization to synthesize the acrylic copolymer.

**3.2. Thermal Analysis.** Thermal properties are critical for PCMs. DSC was used in this research to study the thermal properties of the IPNs. Table 1 exhibits a summary of thermal results for pure PEG and IPN samples. As shown, pristine PEG8000 shows the highest enthalpy of fusion. This result is expected due to the perfection of the crystalline structure in pure PEG. However, synthesizing IPNs out of PU and the acrylic copolymer hinders the free movements of PEG chains and therefore decreases the crystalline structure in the system. The enthalpy of fusion declines, and as shown, IPN50 shows the smallest number in comparison to other IPN samples due to the high percentage of the acrylic copolymer in the system. Crystallization results show the same trends due to the reason mentioned above. IPN90 shows the highest latent heat of fusion with 177.5 J/g, which is still lower than that of pure PEG. However, this number is higher than the reported latent heat of fusion for IPNs and copolymers used in phase change applications. 12,28,56 For instance, Zhou et al. 13 synthesized the PEG4000/MDI/poly(vinyl alcohol) copolymer with a 72.8 J/g enthalpy of fusion and a 61.1 °C transition temperature. Chen synthesized PEG/PU PCMs with the enthalpies of fusion within 103-124 J/g. Sundararajan et al.<sup>23</sup> synthesized PEG8000-based graft semi-IPN. 145 J/g was the highest

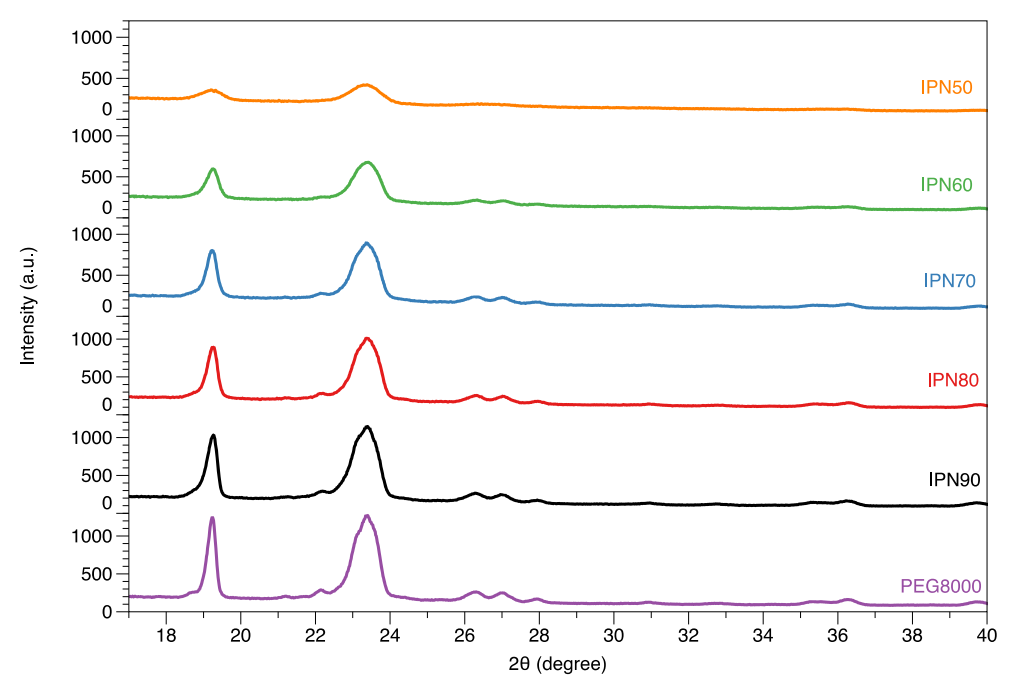


Figure 3. XRD curves of PEG8000 and IPN samples.

Table 2. Mean Size of Crystallites and Percentage of Crystallinity for IPN Samples

sample	mean crystallite size (nm)	crystallinity percentage (%)
PEG8000	19.9	99.6
IPN90	16.8	90.2
IPN80	16.8	71.3
IPN70	16.5	55.2
IPN60	14.6	39.7
IPN50	9.4	24.2
IPN60	14.6	39.7

enthalpy of fusion observed in the paper. Li and Ding<sup>11</sup> fabricated the PEG10000/MDI/PE tertiary copolymer with the highest enthalpy of fusion at 152.97 J/g. Liu et al.<sup>57</sup> also manufactured PEG-based semi-IPN, and the highest enthalpy of fusion obtained in the research was 117 J/g. Su and Liu<sup>55</sup> fabricated PEG10000-based PU with a 138.7 J/g enthalpy of fusion. Finally, Cao and Liu<sup>25</sup> synthesized PEG6000-based hyperbranched PU with a 138.3 J/g enthalpy of fusion. Transition temperatures increase with the PU wt % because

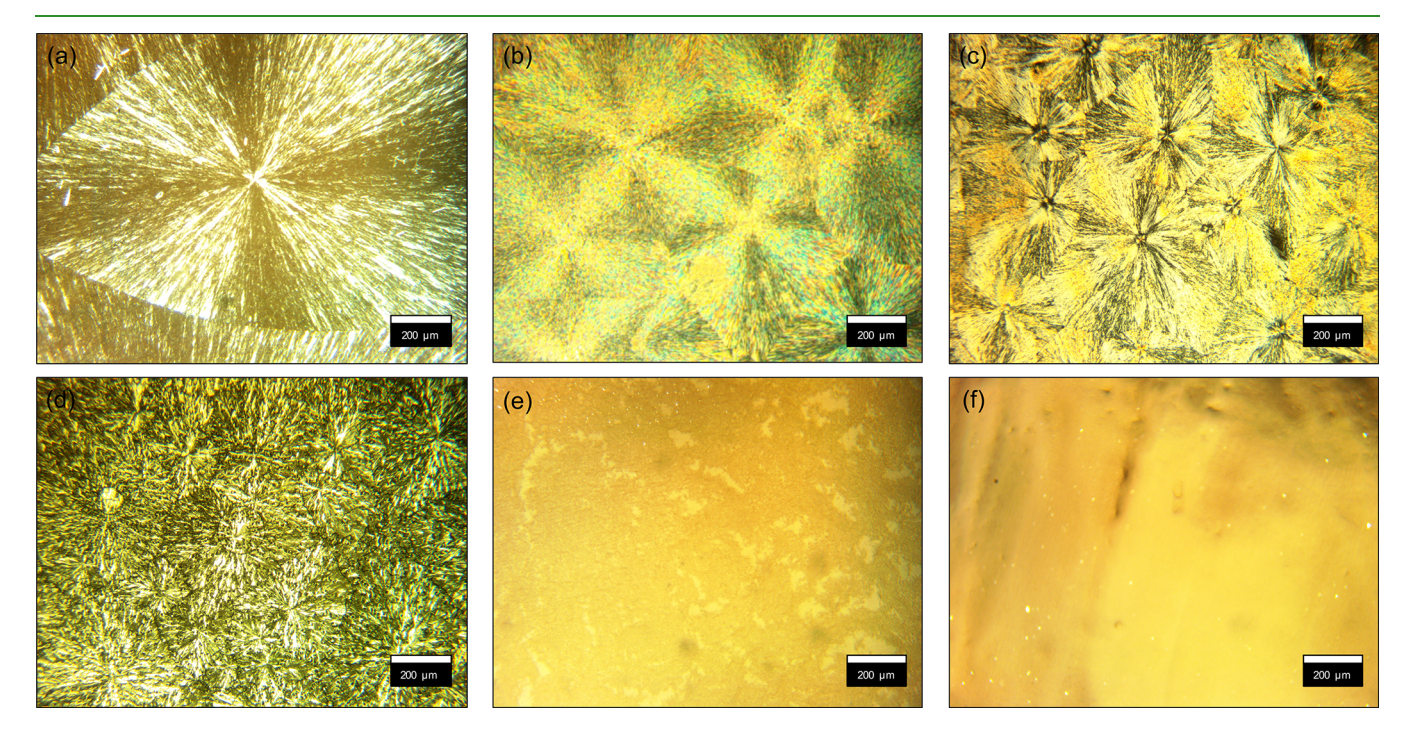


Figure 4. POM photographs of (a) PEG8000 at room temperature, (b) IPN90 at room temperature, (c) IPN80 at room temperature, (d) IPN50 at room temperature, (e) IPN90 at 80 °C, and (f) IPN80 at 80 °C.

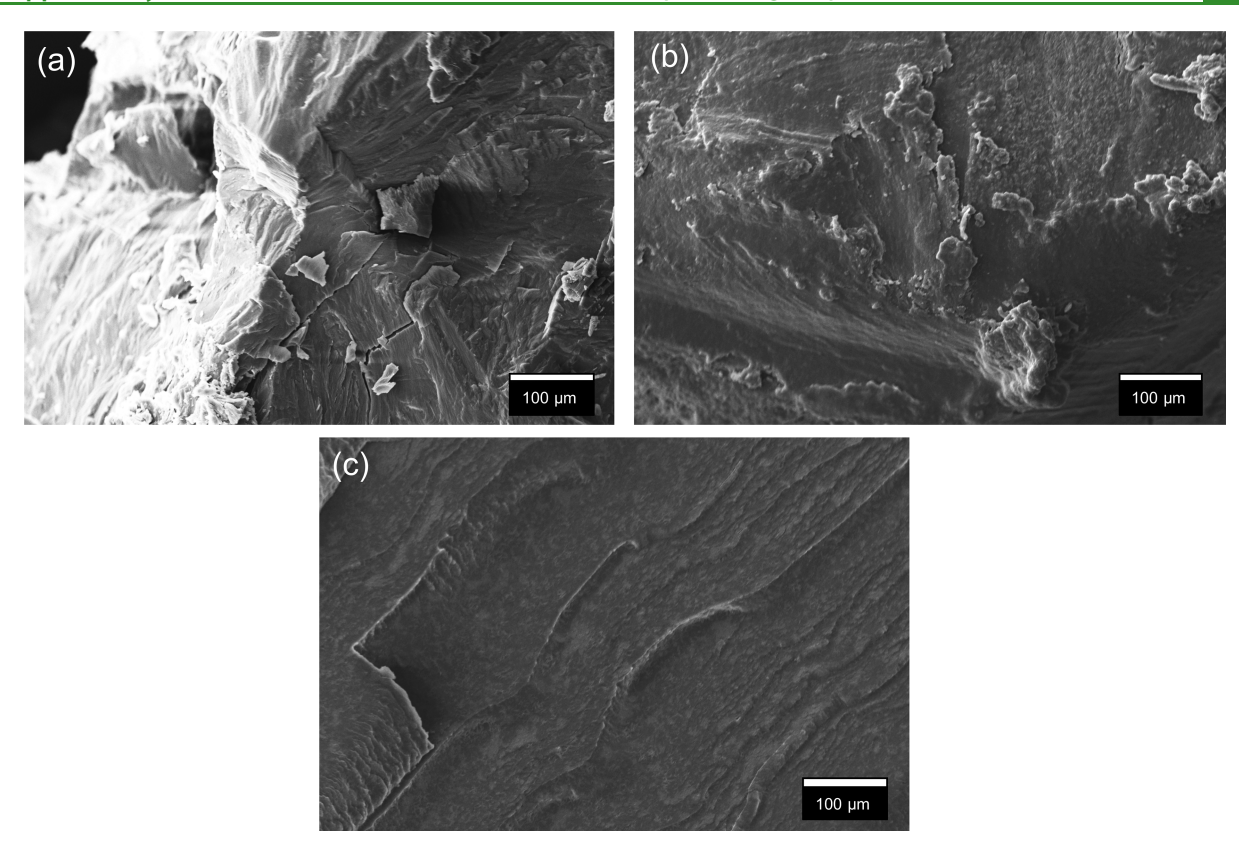


Figure 5. SEM images of (a) IPN90, (b) IPN80, and (c) IPN50.

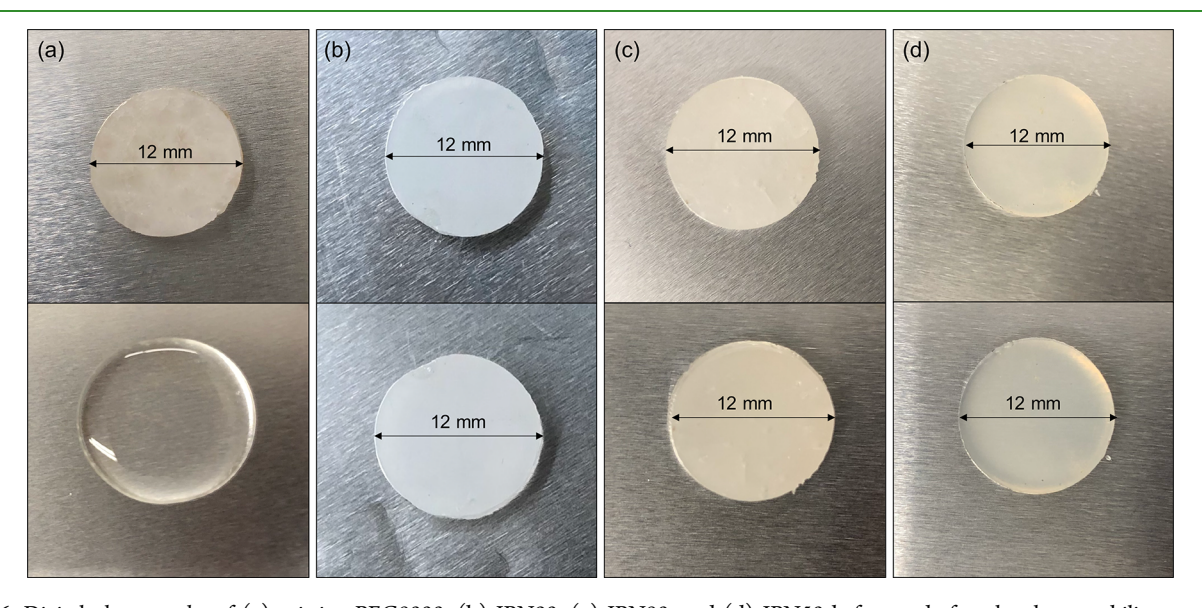


Figure 6. Digital photographs of (a) pristine PEG8000, (b) IPN90, (c) IPN80, and (d) IPN50 before and after the shape stability experiment.

PEG chains have more free volume and mobility to align and make a perfect crystalline structure.

**3.3.** Crystallization Behavior Analysis. XRD was utilized to study the crystallization properties of the samples. Figure 3 shows the diffraction peaks of the samples. As shown, pristine PEG8000 shows the peaks at 19 and 23°, which are characteristic peaks for PEG8000. All IPN samples show a peak at the same diffraction angles, which shows that the crystallization properties of PEG8000 does not change after the synthesis of the IPN samples. However, the height of the peak starts to decrease in IPN90, and it continues to decline by

reducing the amount of PEG in systems. IPN50 shows the lowest height in diffraction peak due to the reduction of PEG in the reactive system and the presence of the acrylic copolymer, which destroys the perfection of the crystallization in PEG. Moreover, although the chemical interaction between the –OH group of PEG and BisGMA with the isocyanate group in DCH brings shape stability into the system, it decreases the perfection of the crystallization even more.<sup>23</sup>

The Scherrer equation (eq 2) was utilized to calculate the mean size of crystallites in IPN samples. Moreover, the

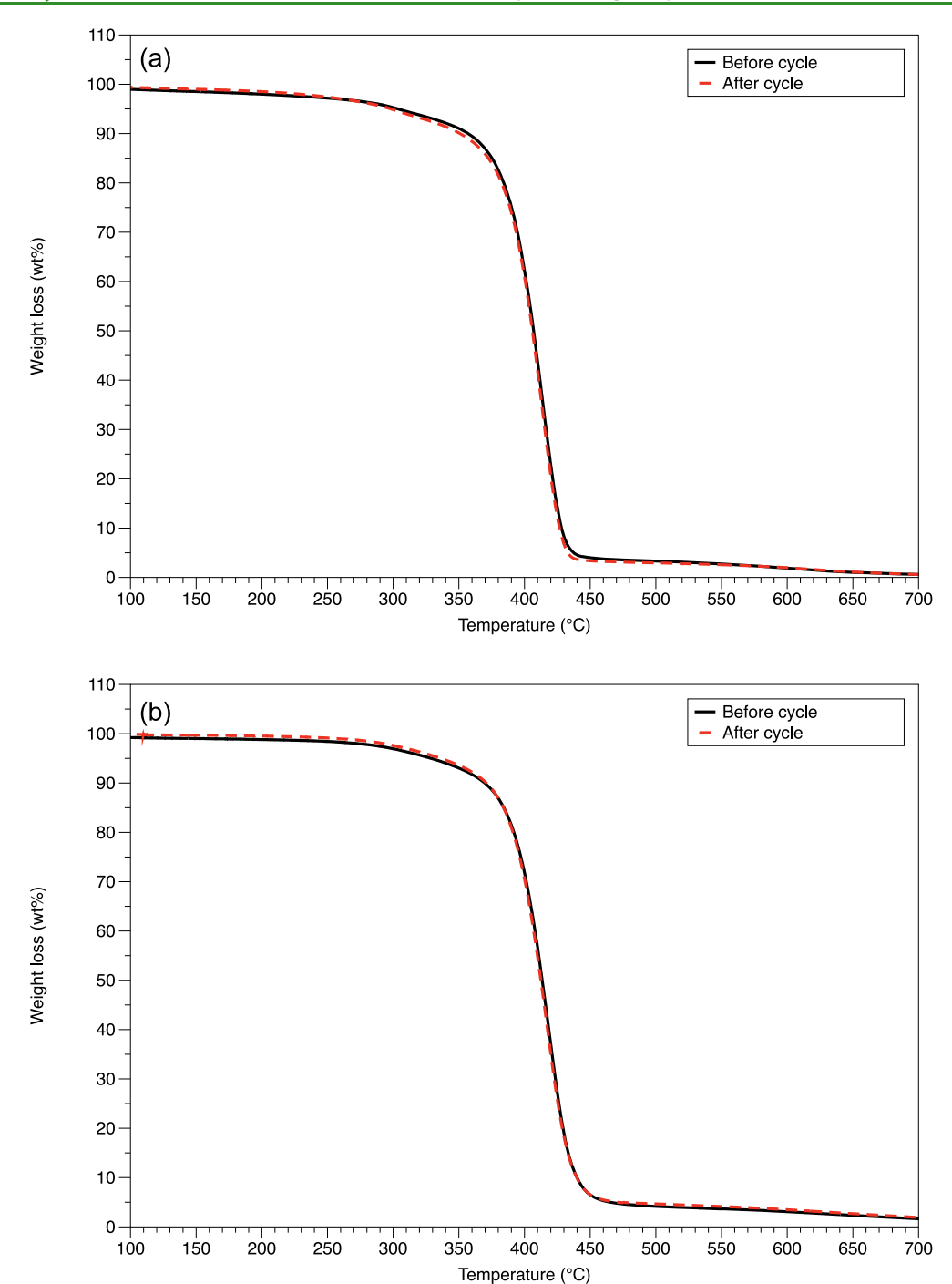


Figure 7. TGA results before and after the thermal cycling test. (a) IPN90 and (b) IPN80.

Table 3. Summary of DSC Results for IPN Samples before and after the Cycling Test

sample		enthalpy of fusion $(\Delta H_{\rm m})$ $(J/g)$	melting temperature $(T_m)$	enthalpy of crystallization $\Delta H_{\rm c}$ $({\rm J/g})$	crystallization temperature $T_{\rm c}$ (°C)
IPN90	before the cycle	177.5	59.9	174.3	43.9
	after the cycle	177.7	60.2	176.6	43.9
IPN80	before the cycle	140.3	59.8	141.4	44.2
	after the cycle	140	60.3	142.9	44.8

percentage of crystallinity for each sample was calculated using eq 1. Table 2 shows a summary of the results.

As shown, the crystallite size and percentage of crystallinity confirm the results from XRD analysis. Pure PEG8000 shows the most significant crystallite size and crystallinity percentage.

The crystallite size and crystallinity percentage start to decrease by adding the acrylic copolymer to form the IPN network, as is expected.

The crystalline morphology of the samples was studied using POM. Figure 4 shows the photograph of the pristine PEG8000

(Figure 4a), IPN samples at room temperature (Figure 4b-d), and IPN samples at 80 °C (Figure 4e,f). As shown, pristine PEG and IPN samples exhibit similar spherulitic crystalline structures. This fact indicates that the crystalline structure of PEG8000 in IPN samples does not change.

Furthermore, the crystallite size becomes smaller by adding more acrylic copolymer to the system due to a decrease in the amount of PEG8000 and the presence of the acrylic copolymer, which acts as a hindrance in IPN samples, therefore destroying the perfection of the PEG crystallization. The crystalline structure of the IPN samples at 80 °C faded away due to the crystalline structure's disappearance at higher temperatures. In other words, the crystalline structure of PEG8000 in the IPN structure was transformed into an amorphous structure. This fact is due to the free movements of PEG8000 chains at 80 °C, which therefore do not align to make the crystalline structure. POM images confirm the results from XRD analysis.

Figure 5 shows the SEM images of fractured IPN samples. As shown, IPN50 (Figure 5c) shows the flat surface with ductile behavior on fractured samples. However, the surface starts to show brittle failure with cracks all over the surfaces by adding more PU to the system due to higher crystallization (Figure 5a,b). Higher crystallization and alignment of chains in IPN90 and IPN80 increase the brittle behavior of the IPN samples. However, the presence of more amorphous regions with many chains entangled in each other is the reason for ductile behavior in the fractured surface of IPN50. SEM images support DSC, XRD, and POM results, indicating higher crystallization by increasing wt % of PU into the IPN system.

3.4. Shape Stability Analysis. IPN samples were put on the 80 °C hot plate for 30 min to examine the shape stability. Figure 6 shows the digital photographs of the pristine PEG8000, IPN90, IPN80, and IPN50 before (first row) and after (second row) of the shape stability experiment. PEG8000 loses its shape immediately after reaching 80 °C and starts to flow because of passing its melting point. In contrast, IPN samples maintain their shape even after 30 min at 80 °C. The presence of the cross-linked acrylic copolymer phase in graft semi-IPN and chemical bonds between the hydroxyl group of PEG and BisGMA with the isocyanate group in DCH, which act as a boundary and trapped long chains of PEG8000, are the reasons behind excellent shape stability of the IPN samples even at a temperature higher than the melting point of PEG8000. It should be added that the transparency of the IPN50 sample is higher than that of other IPN samples. The transparency starts to decrease by adding more PU into the system due to the crystallization increase, as mentioned before.

**3.5. Thermal and Cycling Stability.** Cycling stability is a critical property in PCMs. TGA results before and after cycling experiments for IPN90 and IPN80 are shown in Figure 7. As shown, the degradation process for samples starts at around 300 °C and ends at about 460 °C. The degradation temperature of IPN samples is much higher than the application temperature for phase change applications. These data are in good agreement with literature works on phase change applications of materials. 11,12,23,28,57 Moreover, TGA results approximately overlap before and after cycling experiments.

Table 3 summarizes DSC results for IPN90 and IPN80 before and after the cycling stability experiment. Table 3 indicates that phase-transition temperatures and enthalpies are

very close before and after 25 times of melt-freeze-melt cycles.

FTIR results for IPN90 and IPN80 before and after the thermal cycling revealed good overlap, as shown in Figure S1. This implies that the chemical structure for IPN samples does not change after the thermal cycling experiment.

Furthermore, Figure S2 shows the XRD analysis results for IPN90 and IPN80 before and after the thermal cycling experiment. Good overlap was observed with a small drop in peak intensities in both samples. The mean crystallite sizes for IPN90 and IPN80 after thermal cycling are 15.6 and 15.8 nm, respectively, which are close to their crystallite size before thermal cycling (16.8 nm for both). These findings confirm the FTIR, TGA, and DSC results and indicate excellent thermal cycling stability of the IPN samples.

The contact angle and hydrophilicity of the IPN sample surfaces after thermal cycling were checked. IPN90 and IPN80 showed  $29.1 \pm 4.0$  and  $22.2 \pm 1.9$  contact angles with UPW, respectively. The low contact angle in both IPN samples indicates high hydrophilicity of the samples due to urethane groups in PU and esters in the acrylic copolymer.

### 4. CONCLUSIONS

Graft semi-IPNs with the high latent heat of fusion were synthesized in this research. Chemical bonds between two polymers were used to enhance the compatibility between two phases and improve the shape stability of the IPNs. PEG-based PU is the polymer phase with high latent heat, while the acrylic copolymer acts as a skeleton to keep the whole structure together even at a temperature higher than the melting point of PEG8000. FTIR spectra of IPN samples confirm the successful polymerization of both phases. DSC results show excellent enthalpies higher than other literature values with a proper phase-transition temperature. TGA indicates excellent thermal stability for IPN samples, which is required for phase change applications. XRD analysis and POM images show that the crystalline properties of PEG8000 does not change after the synthesis of IPNs. However, the latent heat and phasetransition temperature become smaller by adding more acrylic copolymer to the system due to a decrease in crystal size and perfection. IPNs exhibit excellent shape stability at 80 °C in comparison to pure PEG8000, which starts to flow immediately after reaching 80 °C. Finally, excellent cycling stability with overlap between DSC, TGA, FTIR, and XRD results before and after cycling experiments was observed. Overall, synthesized IPN shows promising results required in a wide variety of phase change applications.

## ASSOCIATED CONTENT

# Supporting Information

The Supporting Information is available free of charge at https://pubs.acs.org/doi/10.1021/acsapm.0c01363.

FTIR and XRD results before and after the thermal cycling experiment (PDF)

# AUTHOR INFORMATION

# **Corresponding Author**

Maria L. Auad – Department of Chemical Engineering, Auburn University, Auburn, Alabama 36849, United States; Center for Polymers and Advanced Composites, Auburn University, Auburn, Alabama 36849, United States; orcid.org/0000-0001-6932-5645; Email: mla0001@auburn.edu

#### **Authors**

Nima Alizadeh — Department of Chemical Engineering, Auburn University, Auburn, Alabama 36849, United States; Center for Polymers and Advanced Composites, Auburn University, Auburn, Alabama 36849, United States; orcid.org/0000-0002-1396-8358

Royall M. Broughton – Department of Mechanical Engineering and Center for Polymers and Advanced Composites, Auburn University, Auburn, Alabama 36849, United States

Complete contact information is available at: https://pubs.acs.org/10.1021/acsapm.0c01363

#### **Author Contributions**

The manuscript was written through the contributions of all authors. All authors have given their approval to the final version of the document.

#### Notes

The authors declare no competing financial interest.

#### ACKNOWLEDGMENTS

This work was supported by NSF-CREST Center for Sustainable Lightweight Materials (C-SLAM) award #1735971.

#### REFERENCES

- (1) Zalba, B.; Marín, J. M.; Cabeza, L. F.; Mehling, H. Review on thermal energy storage with phase change: materials, heat transfer analysis and applications. *Appl. Therm. Eng.* **2003**, 23, 251–283.
- (2) Khan, Z.; Khan, Z.; Ghafoor, A. A review of performance enhancement of PCM based latent heat storage system within the context of materials, thermal stability and compatibility. *Energy Convers. Manage.* **2016**, *115*, 132–158.
- (3) Abhat, A.; Aboul-Enein, S.; Malatidis, N. A. Heat-of-Fusion Storage Systems for Solar Heating Applications. In *Thermal Storage of Solar Energy*; den Ouden, C., Ed.; Springer Netherlands: Dordrecht, 1981; pp 157–171.
- (4) Ismail, K. A. R.; Henríquez, J. R. Thermally effective windows with moving phase change material curtains. *Appl. Therm. Eng.* **2001**, 21, 1909–1923.
- (5) Vakilaltojjar, S. M.; Saman, W. Analysis and modelling of a phase change storage system for air conditioning applications. *Appl. Therm. Eng.* **2001**, *21*, 249–263.
- (6) Bédécarrats, J. P.; Strub, F.; Falcon, B.; Dumas, J. P. Phase-change thermal energy storage using spherical capsules: performance of a test plant. *Int. J. Refrig.* **1996**, *19*, 187–196.
- (7) Espeau, P.; Mondieig, D.; Haget, Y.; Cuevas-Diarte, M. A. "Active" Package for Thermal Protection of Food Products. *Packag. Technol. Sci.* **1997**, *10*, 253–260.
- (8) Salyer, I. O.; Sircar, A. K. Phase Change Katerials For Heating And Cooling Of Residential Buildings And Other Applications. *Proceedings of the 25th Intersociety Energy Conversion Engineering Conference*, Aug 12–17, 1990; Vol. 1990; pp 236–241.
- (9) Pal, D.; Joshi, Y. Application Of Phase Change Materials For Passive Thermal Control Of Plastic Quad Flat Packages: A Computational Study. *Numer. Heat Transfer, Part A* **1996**, 30, 19–34.
- (10) Mulligan, J. C.; Colvin, D. P.; Bryant, Y. G. Microencapsulated phase-change material suspensions for heat transfer in spacecraft thermal systems. *J. Spacecr. Rockets* **1996**, 33, 278–284.
- (11) Li, W.-D.; Ding, E.-Y. Preparation and characterization of cross-linking PEG/MDI/PE copolymer as solid-solid phase change heat storage material. *Sol. Energy Mater. Sol. Cells* **2007**, *91*, 764–768.

- (12) Sarı, A.; Alkan, C.; Biçer, A. Synthesis and thermal properties of polystyrene-graft-PEG copolymers as new kinds of solid—solid phase change materials for thermal energy storage. *Mater. Chem. Phys.* **2012**, 133, 87—94.
- (13) Zhou, X.-M. Preparation and characterization of PEG/MDI/PVA copolymer as solid-solid phase change heat storage material. *J. Appl. Polym. Sci.* **2009**, *113*, 2041–2045.
- (14) Al-Ahmed, A.; Sarı, A.; Mazumder, M. A. J.; Hekimoğlu, G.; Al-Sulaiman, F. A. Inamuddin, Thermal energy storage and thermal conductivity properties of Octadecanol-MWCNT composite PCMs as promising organic heat storage materials. *Sci. Rep.* **2020**, *10*, 9168.
- (15) Al-Ahmed, A.; Sarı, A.; Mazumder, M. A. J.; Salhi, B.; Hekimoğlu, G.; Al-Sulaiman, F. A. Inamuddin, Thermal energy storage and thermal conductivity properties of fatty acid/fatty acid-grafted-CNTs and fatty acid/CNTs as novel composite phase change materials. *Sci. Rep.* **2020**, *10*, 15388.
- (16) Nazir, H.; Batool, M.; Bolivar Osorio, F. J.; Isaza-Ruiz, M.; Xu, X.; Vignarooban, K.; Phelan, P.; Inamuddin; Kannan, A. M. Recent developments in phase change materials for energy storage applications: A review. *Int. J. Heat Mass Transfer* **2019**, *129*, 491–523.
- (17) Comtois, E.; Favis, B. D.; Dubois, C. Phase transitions and mechanical properties of nitrocellulose plasticized by glycidyl azide polymer and nitroglycerine. *Polym. Eng. Sci.* **2020**, *60*, 2301–2313.
- (18) Sarı, A.; Alkan, C.; Altıntaş, A. Preparation, characterization and latent heat thermal energy storage properties of micronanoencapsulated fatty acids by polystyrene shell. *Appl. Therm. Eng.* **2014**, 73, 1160–1168.
- (19) Xiao, X.; Zhang, P.; Li, M. Preparation and thermal characterization of paraffin/metal foam composite phase change material. *Appl. Energy* **2013**, *112*, 1357–1366.
- (20) Schiffres, S. N.; Harish, S.; Maruyama, S.; Shiomi, J.; Malen, J. A. Tunable Electrical and Thermal Transport in Ice-Templated Multilayer Graphene Nanocomposites through Freezing Rate Control. *ACS Nano* **2013**, *7*, 11183–11189.
- (21) Gunasekara, S. N.; Pan, R.; Chiu, J. N.; Martin, V. Polyols as phase change materials for surplus thermal energy storage. *Appl. Energy* **2016**, *162*, 1439–1452.
- (22) Farid, M. M.; Khudhair, A. M.; Razack, S. A. K.; Al-Hallaj, S. A review on phase change energy storage: materials and applications. *Energy Convers. Manage.* **2004**, *45*, 1597–1615.
- (23) Sundararajan, S.; Samui, A. B.; Kulkarni, P. S. Interpenetrating phase change polymer networks based on crosslinked polyethylene glycol and poly(hydroxyethyl methacrylate). *Sol. Energy Mater. Sol. Cells* **2016**, *149*, 266–274.
- (24) Sari, A.; Alkan, C.; Doguscu, D. K.; Bicer, A. Micro/nano-encapsulated n-heptadecane with polystyrene shell for latent heat thermal energy storage. Sol. Energy Mater. Sol. Cells 2014, 126, 42–50.
- (25) Cao, Q.; Liu, P. Hyperbranched polyurethane as novel solid-solid phase change material for thermal energy storage. *Eur. Polym. J.* **2006**, *42*, 2931–2939.
- (26) Hong, Y.; Xin-shi, G. Preparation of polyethylene—paraffin compound as a form-stable solid-liquid phase change material. *Sol. Energy Mater. Sol. Cells* **2000**, *64*, 37–44.
- (27) Sarı, A. Form-stable paraffin/high density polyethylene composites as solid—liquid phase change material for thermal energy storage: preparation and thermal properties. *Energy Convers. Manage.* **2004**, *45*, 2033–2042.
- (28) Zhang, Y.; Xiu, J.; Tang, B.; Lu, R.; Zhang, S. Novel semi-interpenetrating network structural phase change composites with high phase change enthalpy. *AIChE J.* **2018**, *64*, 688–696.
- (29) Sperling, L. H.; Mishra, V. The current status of interpenetrating polymer networks. *Polym. Adv. Technol.* **1996**, *7*, 197–208.
- (30) Sperling, L. H. Interpenetrating Polymer Networks and Related Materials; Plenum Press: New York, 1981; Vol. 12 (1).
- (31) Li, B.; Bi, X.; Zhang, D.; Whang, F. Forced Compatibility and Mutual Entanglements in Poly (Vinyl Acetate)/Poly (Methyl Acrylate) IPNs. Technomic Publishing Company. *Adv. Interpenetrating Polym. Networks* 1989, 1, 203–220.

- (32) Boudenne, A.; Ibos, L.; Candau, Y. Handbook of Multiphase Polymer Systems; John Wiley & Sons, Ltd., 2011.
- (33) Sperling, L. H. Interpenetrating Polymer Networks: An Overview. *American Chemical Society* **1994**, 239, 3–38.
- (34) Mita, I.; Akiyama, S.., Molecular Design of Network Polymers. In *Macromolecular Design of Polymeric Materials*; Marcel Dekker, Inc., 1997; p 400.
- (35) Chen, C.-H.; Chen, W.-J.; Chen, M.-H.; Li, Y.-M. Simultaneous full-interpenetrating polymer networks of blocked polyurethane and vinyl ester Part I. Synthesis, swelling ratio, thermal properties and morphology. *Polymer* **2000**, *41*, 7961–7967.
- (36) Fan, L. H.; Hu, C. P.; Ying, S. K. Thermal analysis during the formation of polyurethane and vinyl ester resin interpenetrating polymer networks. *Polymer* **1996**, *37*, 975–981.
- (37) Dave, V. J.; Patel, H. S. Synthesis and characterization of interpenetrating polymer networks from transesterified castor oil based polyurethane and polystyrene. *J. Saudi Chem. Soc.* **2017**, 21, 18–24.
- (38) Sundaram, B. M.; Mendez, R. B.; Auad, M. L.; Tippur, H. V. Quasi-static and dynamic mechanical behavior of transparent graft-interpenetrating polymer networks (graft-IPNs). *Polym. Test.* **2018**, 70, 348–362.
- (39) Alizadeh, N.; Thorne, D. P.; Auad, M. L.; Celestine, A. D. N. Mechanical performance of vinyl ester-polyurethane interpenetrating polymer network composites. *J. Appl. Polym. Sci.* **2021**, *138*, 50411.
- (40) Bird, S. A.; Clary, D.; Jajam, K. C.; Tippur, H. V.; Auad, M. L. Synthesis and characterization of high performance, transparent interpenetrating polymer networks with polyurethane and poly(methyl methacrylate). *Polym. Eng. Sci.* 2013, 53, 716–723.
- (41) Ballestero, R.; Sundaram, B. M.; Tippur, H. V.; Auad, M. L. Sequential graft-interpenetrating polymer networks based on polyurethane and acrylic/ester copolymers. *eXPRESS Polym. Lett.* **2016**, *10*, 204–215.
- (42) Alizadeh, N.; Barde, M.; Minkler, M.; Celestine, A.-D.; Agrawal, V.; Beckingham, B.; Auad, M. L. High-fracture-toughness acrylic—polyurethane-based graft-interpenetrating polymer networks for transparent applications. *Polym. Int.* **2020**, DOI: 10.1002/pi.6149.
- (43) Jajam, K. C.; Bird, S. A.; Auad, M. L.; Tippur, H. V. Tensile, fracture and impact behavior of transparent Interpenetrating Polymer Networks with polyurethane-poly(methyl methacrylate). *Polym. Test.* **2013**, 32, 889–900.
- (44) Jajam, K. C.; Tippur, H. V.; Bird, S. A.; Auad, M. L. In Dynamic Fracture and Impact Energy Absorption Characteristics of PMMA-PU Transparent Interpenetrating Polymer Networks (IPNs). *Dynamic Behavior of Materials*; Song, B., Casem, D., Kimberley, J., Eds.; Springer International Publishing: Cham, 2014; , Vol. 1, pp 277–284.
- (45) Jajam, K. C.; Bird, S. A.; Auad, M. L.; Tippur, H. V. Development and Characterization of a PU-PMMA Transparent Interpenetrating Polymer Networks (t-IPNs). In *Dynamic Behavior of Materials*; Proulx, T., Ed.; Springer New York: New York, NY, 2011; , Vol. 1, pp 117–121.
- (46) Méndez, R. B. Sequential Graft-Interpenetrating Polymer Networks Based on Polyurethane and Acrylic/ester Copolymers; Auburn University: Auburn, AL, 2015.
- (47) Hillerström, A.; Andersson, M.; Pedersen, J. S.; Altskär, A.; Langton, M.; van Stam, J.; Kronberg, B. Transparency and wettability of PVP/PDMS-IPN synthesized in different organic solvents. *J. Appl. Polym. Sci.* **2009**, *114*, 1828–1839.
- (48) Alizadeh, N.; Bird, S. A.; Mendez, R. B.; Jajam, K. C.; Alexander, A. C.; Tippur, H. V.; Auad, M. L. Chapter 11-Synthesis and Characterization of High Performance Interpenetrating Polymer Networks With Polyurethane and Poly(methyl methacrylate). In *Unsaturated Polyester Resins*; Thomas, S., Hosur, M., Chirayil, C. J., Eds.; Elsevier, 2019; pp 243–255.
- (49) Qin, C.-L.; Cai, W.-M.; Cai, J.; Tang, D.-Y.; Zhang, J.-S.; Qin, M. Damping properties and morphology of polyurethane/vinyl ester resin interpenetrating polymer network. *Mater. Chem. Phys.* **2004**, *85*, 402–409.

- (50) Bird, S. A. Interpenetrating Polymer Networks with Polyurethane and Methacrylate-Based Polymers; Auburn University: Auburn, AL, 2013
- (51) Alizadeh, N.; Celestine, A.-D. N.; Auad, M. L.; Agrawal, V. Mechanical characterization and modeling stress relaxation behavior of acrylic—polyurethane-based graft-interpenetrating polymer networks. *Polym. Eng. Sci.* **2021**, DOI: 10.1002/pen.25640.
- (52) Huang, J.; Zhang, L. Effects of NCO/OH molar ratio on structure and properties of graft-interpenetrating polymer networks from polyurethane and nitrolignin. *Polymer* **2002**, *43*, 2287–2294.
- (53) Zalipsky, S.; Harris, J. M. Introduction to Chemistry and Biological Applications of Poly(ethylene glycol). *Poly(ethylene glycol)*; American Chemical Society, 1997; Vol. 680, pp 1–13.
- (54) Natta, G.; Corradini, P.; Bassi, I. W. Crystal structure of isotactic polystyrene. *Il Nuovo Cimento* (1955–1965), 1960; Vol. 15 (1), pp 68–82.
- (55) Su, J.-C.; Liu, P.-S. A novel solid—solid phase change heat storage material with polyurethane block copolymer structure. *Energy Convers. Manage.* **2006**, *47*, 3185—3191.
- (56) Jiang, Y.; Ding, E.; Li, G. Study on transition characteristics of PEG/CDA solid—solid phase change materials. *Polymer* **2002**, *43*, 117–122.
- (57) Liu, Z.; Zhang, Y.; Hu, K.; Xiao, Y.; Wang, J.; Zhou, C.; Lei, J. Preparation and properties of polyethylene glycol based semi-interpenetrating polymer network as novel form-stable phase change materials for thermal energy storage. *Energy Build.* **2016**, *127*, 327–336.
- (58) Pielichowski, K.; Flejtuch, K. Differential scanning calorimetry studies on poly(ethylene glycol) with different molecular weights for thermal energy storage materials. *Polym. Adv. Technol.* **2002**, *13*, 690–696.
- (59) Scherrer, P. Nachrichten von der Gesellschaft der Wissenschaften zu Göttingen. *Mathematisch-Physikalische Klasse* **1918**, 2, 98–100.
- (60) Pavia, D. L.; Lampman, G. M.; Kriz, G. S. Introduction to Spectroscopy, 3rd ed.; Thomson Learning: Washington, 2001.
- (61) Chen, C.; Chen, J.; Jia, Y.; Topham, P. D.; Wang, L. Binary shape-stabilized phase change materials based on poly(ethylene glycol)/polyurethane composite with dual-phase transition. *J. Mater. Sci.* **2018**, *53*, 16539–16556.